JOURNAL OF MATERIALS SCIENCE 8 (1973) 1545–1553

A mechanism of surface micro-roughening by ion bombardment

PETER SIGMUND
H. C. Ørsted Institute, DK-2100 Copenhagen Ø, Denmark

The spatial distribution of sputter-etch effects is analysed theoretically under the assumption of random slowing-down of the bombarding ions. When a surface is bombarded at locally oblique incidence the most pronounced sputtering effect is likely to be observed not at the very point of impact, but further "downstream". This effect may cause a significant reduction of the local sputtering yield on top of a spike or a ridge, and an increase on the bottom of a groove or a crater. As a consequence, small irregularities on a relatively smooth surface may be enhanced during bombardment. It is concluded that a microscopically flat surface is unstable under high-dose ion bombardment unless atom migration acts as a dominating smoothing effect. Conversely, sharp cones appear to be surprisingly stable under bombardment. Even on a clean surface, cones erode more slowly than a plane surface, provided that their dimensions are of the order of, or less than, the penetration depth of the ions.

1. Introduction

Ion-bombarded surfaces may exhibit a variety of picturesque structures when viewed by, e.g. scanning electron microscopy or replica techniques [1-3]. Such structures may depend upon the purity of a surface and structural defects like grain boundaries, dislocations etc. Existing experimental evidence has led several groups [4-6] to suggest that surface topography also may occur under bombardment of clean single crystal surfaces, i.e. without a dominating action of pre-existing defects or impurities. The occurrence of craters and cones, hillocks and furrows, ridges and grooves under bombardment may not only be annoying to the technologist who started off to *polish* a surface by ion bombardment, it may also need to be considered in the theory of sputtering, where the assumption of a plane target surface often enters.

In the discussion of radiation-induced surface topography, a major role is being played by the dependence of the sputtering yield on angle of incidence [5, 6], crystallographic orientation [4], and defect state [4]. The implication seems to be that, once a certain structure has nucleated, its growth will largely be determined by the angular dependence of the sputtering yield [5-7], while nucleation takes place at radiation-induced defects [4] or impurities [8]. The underlying assumption is that a flat, homogeneous surface sputters homogeneously, i.e. that *some* significant disturbance must be created before observable structure may occur.

The question may be asked whether a plane surface is a stable equilibrium configuration under ion bombardment. The arguments of Stewart and Thompson [5] suggest a dynamic equilibrium of inclined surface planes, oriented according to maximum sputtering yield, moving rapidly along the surface. The mutual interaction of many such moving planes would then give rise to various observable surface structures. While the experimental results [5, 9] seem to confirm a preferred inclination of surface planes, it appears difficult in this model to explain the existence of cones on top of an otherwise plane, horizontal surface. One would expect the cones to erode much faster than the underlying plane [6]. Catana *et al* [6] suggested a preferred orientation of surface planes at an angle θ_0 where the sputtering yield is $S(\theta_0) = S(0)$, i.e. the yield at normal incidence. Their computer simulations yield a drastic enhancement of a given (sine-like) surface roughness during subsequent bombardment. It appears somewhat easier within such a picture to explain the

© *1973 Chapman and Hall Ltd.*

abundance of cones, palisades, ridges, and furrows reported lately [9-11]. A number of secondary effects that had been omitted in both models have been pointed out more recently [12].

Nucleation has been suggested to take place at radiation-induced defect clusters [4], and there seems to be experimental evidence to support this assertion. It is not obvious whether a similar nucleation mechanism would operate also in amorphous materials [12, 22].

The inherent spatial inhomogeneity of the sputtering process has usually been left out of consideration. In [5 and 6], the sputtering yield enters as a continuous erosion function that depends on the orientation of the surface in the vicinity of any considered point. One neglects the discontinuous character of a sputtering event, the fluctuations in the yield, and the finite dimensions of atomic collision cascades initiated by the bombarding ions. Such a simplification may be justified if one is interested in the *growth* of a surface structure with ultimate dimensions that are much larger than the dimensions of atomic collision cascades. This is often the case (e.g. [7-9]). Some caution may, however, be appropriate in high-energy experiments because of greater penetration [10], or high-resolution experiments [11]. It is less obvious how to justify the neglect of spatial inhomogeneities in explaining the *nucleation* process.

The present study has been undertaken mainly in order to get an indication of whether the assumption of a plane surface in sputtering theory is feasible. It turned out that, on a length scale determined by the penetration depth of the bombarding ions, a planar surface is unstable under ion bombardment unless a separate smoothing process (e.g. atom migration) is acting besides sputtering. The model is based on a theory of sputtering of random targets proposed by the author [13]. The model predicts in a rather direct way a considerable stability of tiny cones and ridges, and appears to be consistent with a number of experimental observations.

It is not suggested that the present model should replace the existing mechanisms to explain the occurrence of surface topography. In view of the great variety of observations, there is probably ample space for many competing mechanisms. The considerations presented in the following two sections can be incorporated readily in a computer simulation model like the one described in [6]. Therefore, in the following discussion we restrict our attention to a small number of instructive and, possibly, oversimplified examples, in order to demonstrate the significance of the effects. Some implications and limitations will be discussed subsequently.

2. The model

Let a collimated, monochromatic ion beam bombard a solid target with a plane surface. The average number of sputtered atoms per bombarding ion, i.e. the total sputtering yield, is then given by [13]

$$S(x) = \Lambda F_D(x) \tag{1}$$

where x is the depth at which sputtering is observed, e.g. the thickness of a foil that can be passed by the ion beam. For a thick target, sputtering can be observed only at $x = 0$. The quantity Λ is a constant characterizing the target material, in particular the state of the surface, and $F_D(x)$ the average energy deposited per unit depth at depth x. This function has been studied in detail in [14], under the assumption of random slowing-down of the ion and the high-energy secondary recoil atoms in an infinite medium. In addition to its depth dependence, $F_D(x)$ also depends on the target/ion mass ratio, ion energy, and angle of incidence.

Straightforward extension of Equation 1 to an arbitrary (non-planar) geometry yields

$$S(\mathbf{r})\mathrm{d}a = \Lambda F_D(\mathbf{r})\,\mathrm{d}a \tag{2}$$

where (Fig. 1) $S(\mathbf{r})\,\mathrm{d}a$ is the average number of target atoms sputtered from a surface element $\mathrm{d}a$ at a vector distance, $\mathbf{r}$, from the point of impact of the bombarding ion, and $F_D(\mathbf{r})$ the energy

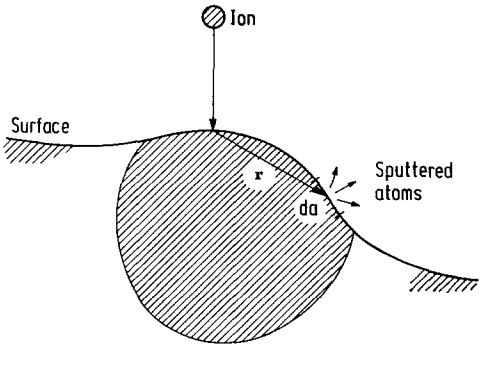

Figure 1 Spatial distribution of the sputtering process. At a vector distance $\mathbf{r}$ from the impact point of the ion, $S(\mathbf{r})\mathrm{d}a$ atoms are sputtered in the average from the area $\mathrm{d}a$.

deposited per unit volume at **r**. For planar geometry we have $da = dydz$, and Equation 1 follows from Equation 2 by means of the relation [14]

$$F_D(x) = \int\int dydz\, F_D(\mathbf{r}) .$$

The method used to derive Equation 1 in [13] is not particularly suited to derive Equation 2. However, Equation 2 can be derived easily by means of the arguments used in [15]. Note, in particular, that the *orientation* of the surface element da does not enter. We call $S(\mathbf{r})$ the *local* or *differential* sputtering yield.

Fig. 2 shows a typical contour plot of $F_D(\mathbf{r})$, together with the ion range, in the x-y plane [14]

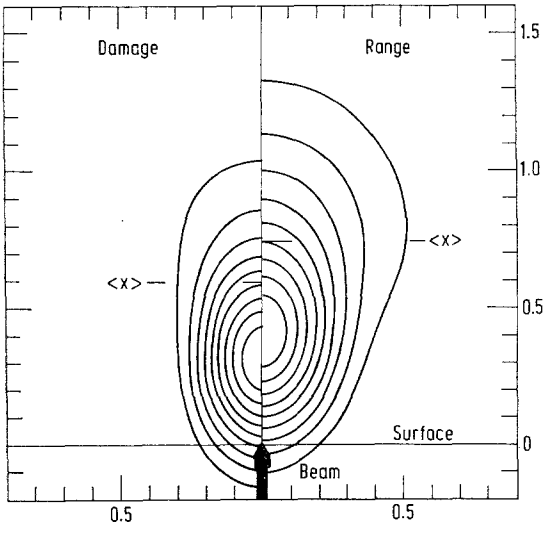

Figure 2 Contour plot of average deposited energy (left) and ion range profile (right), calculated for equal masses of bombarding ion and target (from Winterbon *et al* [14]). Both profiles show cylindrical symmetry around the ion beam direction. Contour interval 10% of maximum. Length in units of the average path length of the ion.

(there is cylindrical symmetry around the x-axis). The scale on the co-ordinate axes depends on ion energy. The difference between successive contours is 10% of the maximum value.

F_D is replotted in Fig. 3, and an intersecting surface plane AB has been included, which contains the z-axis. The angle of incidence of the ion beam with respect to the surface normal is θ. It is seen immediately that the maximum of the deposited-energy function along the surface plane is not in the point of impact, but in a point

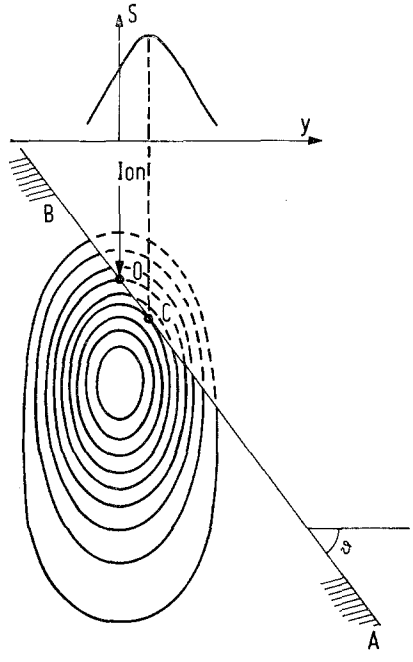

Figure 3 Contour plot of deposited energy as in Fig. 2. Target surface AB, angle-of-incidence ϑ, point of ion impact O and point of maximum sputtering yield C. Upper graph: Distribution of sputtering yield along surface for ion incident at O.

C further "downstream". By use of the contour map the deposited energy $F_D(\mathbf{r})$ can be drawn up as a function of lateral co-ordinate y for $z = 0$. This curve has also been included in Fig. 3. In view of Equation 2, also the local sputtering yield has its maximum in the point C and not in the point of impact. This is a special case of a more general result: because of the initial momentum of the ion, the centre of the deposited-energy distribution is located at a finite distance from the point of impact – seen in the direction of the bombarding ion. Hence there will usually be parts of the sputtered surface that are sufficiently close to the centre to be on a higher contour than the point of impact.

Now let us bombard a surface with a structure of the type sketched in Fig. 4. Assume that the distance between the points A and B, B and C, etc. correspond to the distance OC in Fig. 3. Then, sputtering around the point B is dominated by those ions hitting near A, sputtering around the point C by ions hitting near B, etc. There is little sputtering near A, but more than average in D, since also ions hitting in E con

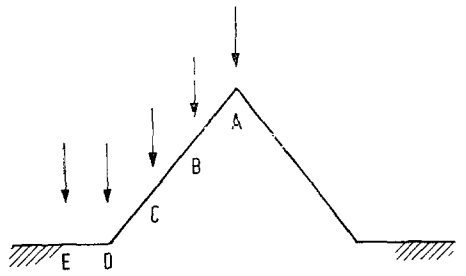

Figure 4 See text.

tribute a little. Again, this is a rather general feature, which could have been sketched qualitatively by using a very differently shaped structure. The main point is that the surface is not plane, so there is a tendency towards less sputtering near a top, and more sputtering near a valley. *Obviously, there is an instability.*

It may be appropriate at this point to mention two of several simplifications that have been made up to now, in addition to the initial assumption of random slowing-down:

(i) we have ignored in Figs. 3 and 4 the possible interruption of a collision cascade by the target surface, and

(ii) we used the statistical average for $F_D(\mathbf{r})$ instead of an energy distribution for an individual cascade.

Some comments will be made to justify these simplifications.

(i) The profiles of Fig. 2 have been calculated for slowing-down in an infinite medium.Introduction of a surface will cause modifications not only of those parts of the cascade that are literally cut away, but also those located near the surface. A correction could be made in principle, provided that such corrections were reasonably small [16]. In the present work we do not aim at high numerical accuracy. Hence, we can apply a rather leisurely criterion for the validity of assuming an infinite medium: contours from maximum down to $\sim \frac{2}{3}$ maximum level must lie in the target, and so must the straight line connecting the point of impact with the cascade centre. In case of Fig. 3, this means that any quantitative conclusions have to be modified for $\theta \gtrsim 60°$. Qualitative conclusions are much less sensitively affected, but may break down in case of grazing incidence, or in the presence of cavities etc. *However, even at grazing incidence the calculated sputtering yield can be applied as an upper limit.*

(ii) The profiles of Fig. 2 are *average* profiles taken over a large number of events with identical initial conditions. Individual cascades may scatter significantly [17]. However, sputtering yields are usually small (less than $\sim$ 10 atoms per ion), so that surface changes, except on an atomic scale, necessarily require a great number of impinging ions. Considerably higher sputtering yields ($\sim$ 100 or more) can be achieved by using *very heavy* ions. In these cases, however, cascades show less fluctuation [17]. For these two reasons, the use of average cascade profiles appears to be justified normally. (The statement will be modified slightly in Section 4.)

3. Calculations

Let a homogeneous beam of total fluence ϕ [ions cm^{-2}] strike a surface A along the x-direction (Fig. 5). An ion hitting the surface in a

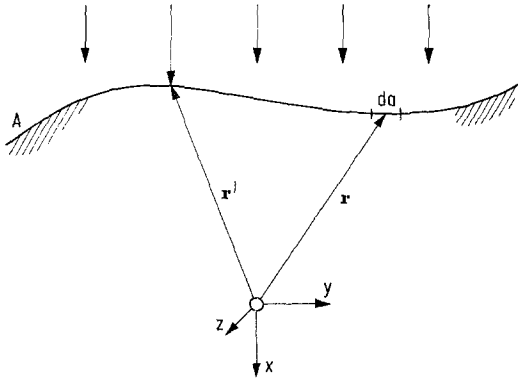

Figure 5 Sputtering of a surface A by a homogeneous ion beam. Impact in $\mathbf{r}'$, sputtering from da at $\mathbf{r}$. Cartesian co-ordinate system with the x-axis parallel to the beam.

point $\mathbf{r}'$ causes a number of atoms to be sputtered from an area da at $\mathbf{r}$. This number is given by $\Lambda F_D(\mathbf{r} - \mathbf{r}')\,da$, in the average, according to Equation 2. Hence, the total number of atoms sputtered from the area da at $\mathbf{r}$ is given by

$$N_S(\mathbf{r})\,da = \phi\,\Lambda\,da \int\int_A dy'\,dz'\,F_D(\mathbf{r} - \mathbf{r}') \qquad (3)$$

where $\phi\,dy'\,dz'$ is the number of ions hitting an area $dy'\,dz'$.

The target surface is determined by some relation

$$x = f(y, z)\,; \quad x' = f(y', z')\,. \qquad (4)$$

For a single-valued function $x = f(y, z)$, this representation leaves no ambiguities with respect

to the magnitude of the particle flux bombarding individual parts of the surface*.

Since Equation 3 can be incorporated easily in a computer simulation program like that of [6], we restrict our attention to the evaluation of a few simple examples. We first look at a 1-dimensional problem, i.e. a furrow or ridge rather than a crater or a peak. The following surface, consisting of two intersecting planes, contains a number of interesting limiting cases,

$$\begin{aligned} x = &- C_1 y \ldots y < 0 \\ &C_2 y \ldots y > 0 . \end{aligned} \tag{5}$$

For C_1, $C_2 > 0$ we have a ridge, and for C_1, $C_2 < 0$, a furrow. We approximate the deposited-energy profile by a Gaussian [14], i.e.

$$F_D(x, y) = \int_{-\infty}^{\infty} dz\, F_D(\mathbf{r}) = \frac{\nu}{2\pi\,\alpha\,\beta}\, e^{-(x-a)^2/(2\alpha^2)-y^2/(2\beta^2)} \tag{6}$$

where ν is the total energy deposited in atomic motion [18].

Numerical values of the average energy deposition depth a and the longitudinal and lateral widths α and β can be found in [14]. Usually all three quantities are of the order of the ion range. Note that the Gaussian approximation has been found to be sufficient in most situations discussed in connection with calculations of the sputtering yield [13].

Inserting Equations 5 and 6 into Equation 3 and integrating, we obtain

$$N_S(\mathbf{r})\, da = \phi\, \Lambda\, da \frac{\nu}{\sqrt{(2\pi)}} \tfrac{1}{2}\left\{\frac{e^{B_1}}{A_1}\operatorname{erfc}(D_1) + \frac{e^{B_2}}{A_2}\operatorname{erfc}(D_2)\right\} \tag{7}$$

where

$$A_1 = \sqrt{(\beta^2 C_1^2 + \alpha^2)}\ ; \quad A_2 = \sqrt{(\beta^2 C_2^2 + \alpha^2)}$$

$$B_1 = -\tfrac{1}{2}\frac{(x - a + C_1 y)^2}{A_1^2}\ ; \qquad B_2 = -\tfrac{1}{2}\frac{(x - a - C_2 y)^2}{A_2^2}$$

$$D_1 = -\frac{C_1 \beta^2 (x - a) - y\alpha^2}{\alpha\beta\sqrt{2}\, A_1}\ ; \qquad D_2 = -\frac{C_2 \beta^2 (x - a) + y\alpha^2}{\alpha\beta\sqrt{2}\, A_2} \tag{8}$$

and

$$\operatorname{erfc}(x) = \frac{2}{\sqrt{\pi}}\int_x^{\infty} dt\, e^{-t^2} .$$

Let us first consider a symmetric ridge ($C_1 = C_2 > 0$). We can compare the sputtered intensity near the top of the ridge ($x = y = 0$) with the intensity far away ($y \to +\infty$). From Equation 7, we obtain

$$N_S(0)\, da = \phi\, \Lambda\, da \frac{\nu}{\sqrt{(2\pi)}} \frac{e^{-a^2/(2A_1^2)}}{A_1} \operatorname{erfc}(D_1)$$

$$N_S(\infty)\, da = \phi\, \Lambda\, da \frac{\nu}{\sqrt{(2\pi)}} \frac{e^{-a^2/(2A_1^2)}}{A_1} .$$

Hence,

$$\frac{N_S(0)\, da}{N_S(\infty)\, da} = \operatorname{erfc}\left(\frac{C_1\, a\, \beta}{\alpha\sqrt{2}\, A_1}\right) ; \quad C_1 = C_2 . \tag{9}$$

This is smaller than 1, as expected (note that $\operatorname{erfc}(0) = 1$). For a symmetric furrow, Equation 9 remains valid, but $C_1 < 0$, so the ratio becomes greater than 1.

A rough orientation over the magnitude of the effect is found by assuming a spherically symmetric profile, i.e. $\alpha = \beta$. With an opening angle 2ψ of the ridge (Fig. 6a), we have $C_1 = \cot\psi$, so

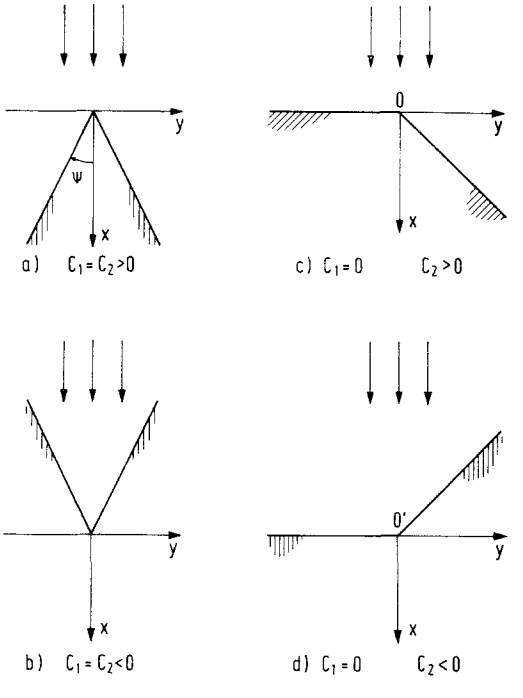

Figure 6 Four characteristic situations comprised by Equation 7. See text.

* The author thanks Dr I. Teodorescu for warning him against the treacheries of various cosine factors.

$$\frac{N_S(0)\,da}{N_S(\infty)\,da} = \operatorname{erfc}\left(\frac{a}{\alpha\sqrt{2}}\cos\psi\right);\ \text{for } \alpha = \beta. \quad (9a)$$

Since typical values of the ratio α/a lie in the region [14] ~ 0.5 to 1.5, the argument in the error function can become as large as ~ 1, and this may in turn result in a near order-of-magnitude reduction of the sputtering yield on top of a ridge according to Equation 9a. With the data of Winterbon, Sigmund, and Sanders [14], and $\psi = 45°$, the ratio (Equation 9) assumes the values quoted in Table I.

TABLE I Ratio (Equation 9) between sputtering rates per unit surface area near the top of a ridge (opening angle $2\psi = 90°$) and an inclined plane at 45°. Input parameters from Winterbon *et al* [14]. M_1 = ion mass; M_2 = target mass; m = exponent in power cross-section. The situation corresponds approximately to Fig. 4 for the ratio $N_S(A)/N_S(C)$.

m	M_2/M_1		
	$\frac{1}{4}$	1	4
$\frac{1}{3}$	0.355	0.354	0.440
$\frac{1}{2}$	0.413	0.381	0.401

We note that Equation 9 takes on a limiting value $\operatorname{erfc}(a/\alpha\sqrt{2})$ for a very steep ridge ($\psi \to 0$) This will be an *overestimation* of the actual ratio because of the breakdown of the assumption of an infinite medium.

Another interesting quantity is the ratio between the sputtering yield on top of a ridge and that of a horizontal plane ($C_1 = C_2 = 0$). Equation 7 yields for this ratio

$$\frac{N_S(\text{ridge})\,da}{N_S(\text{plane})\,da} = \frac{\alpha}{A_1}\,e^{(a^2/2)\,(1/\alpha^2 - 1/A_1^2)} \operatorname{erfc}\left(\frac{C_1\,\beta\,a}{\alpha\sqrt{2}\,A_1}\right). \quad (10)$$

In the limiting case of a narrow ridge (small ψ), this reads

$$\frac{N_S(\text{ridge})\,da}{N_S(\text{plane})\,da} \sim \sin\psi \cdot \frac{\alpha}{\beta}\,e^{a^2/2\alpha^2} \operatorname{erfc}\left(\frac{a}{\alpha\sqrt{2}}\right) \quad \text{for small } \psi. \quad (10a)$$

If we divide Equation 10 or 10a by the factor $\sin\psi$, we get the ratio of the *regression speeds* of the two surfaces *in the direction of the beam* [6]. Evaluating this remaining expression in the cases mentioned in Table I we obtain the values quoted in Table II. Again, these values *overestimate* the actual ratio, since the effect of a finite surface has a greater influence on the sputtering of a narrow ridge than on that of a plane at perpendicular incidence. Hence, we conclude that the regression speed of the top of a ridge is substantially smaller than that of a planar surface perpendicular to the beam, even for a relatively large opening angle ($\psi = 45°$).

TABLE II Ratio between the regression speeds in the beam direction of the area around the top of a ridge (opening angle 2ψ) and a horizontal plane. Same input data as in Table I. The ratio has been found by dividing Equation 10 by $\sin\psi$.

m	M_2/M_1		
	$\frac{1}{4}$	1	4
$\frac{1}{3}$	0.643	0.619	0.628
$\frac{1}{2}$	0.685	0.666	0.606

Before a conclusion can be made on the stability of a ridge as compared with that of a plane, we need an estimate of the size of the region where the sputtering yield is smaller than normal. We evaluate only the most critical case, i.e. that of a very steep ridge, $C_1 \sim (1/\sin\psi) \to \infty$ In this limit, we obtain from Equation 7

$$N_S\,da \sim \phi\,\Lambda\,da\,\frac{\nu}{\sqrt{(2\pi)}}\,\frac{\sin\psi}{\beta}\operatorname{erfc}\left(-\frac{x-a}{\alpha\sqrt{2}}\right)\cdot \tfrac{1}{2}(1 + e^{-2y^2/\beta^2});\quad C_1 = C_2 \gg 1 \quad (11)$$

where x is the depth measured from the top of the ridge, and y the lateral co-ordinate of the surface. It is seen that the factor $\operatorname{erfc}[-(x-a)/\alpha\sqrt{2}]$ increases monotonically with increasing x with a characteristic depth of $x \sim a$, the average energy deposition depth, while the second factor decreases monotonically with increasing y and a characteristic width of $y \sim \beta$. Obviously, for $y \gtrsim \beta$ ions hitting on one side of the ridge do not appreciably sputter atoms on the other side.

We conclude from Equations 10 and 11 that a steep ridge with a height of the order of the energy deposition depth ($\approx$ penetration depth [14]) is more stable against sputtering than a planar surface facing the beam at a right angle.

As mentioned previously, the corresponding relations for the groove (Fig. 6b) are found by using negative values of C_1 in Equations 9 and 10, or changing sign in the arguments of the error functions in Equations 9a, 10a and 11. A substantial increase of the sputtering yield near the bottom of a groove would be predicted from

these equations. However, the physical significance of such numbers is somewhat doubtful, since many of the atoms sputtered near the bottom of a narrow groove will have a chance to be re-collected on the opposite wall.

Another interesting case is that of a slope adjacent to a plateau (Fig. 6c). Setting $C_1 = 0$ in Equation 7, but $C_2 \neq 0$, we immediately obtain the sputtering yields in the points O and O' as the arithmetic means of the yields of the plane and that of a ridge or groove with the same slope. Hence, we get qualitatively the same effects as previously but less pronounced. This may have the result that the edge of a plateau develops to become a ridge. Also, at the bottom of a slope that ends up in the plane (Fig. 6d), a groove may develop. The latter effect is well known from the experimental observations, and alternative explanations involving scattered ions or high-energy sputtered atoms have been offered [9, 12]. Fig. 7 shows a

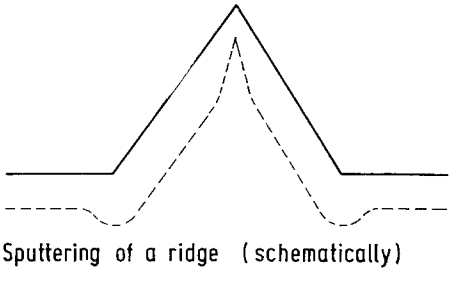

Figure 7 Sputtering of a ridge (schematically). The regression speed is greatest at the lower edge, slightly smaller on the slope, considerably smaller on the horizontal plane, and smallest near the top.

qualitative sketch of the development of a ridge located on a plane surface, according to the results obtained so far.

We now proceed to a two-dimensional situation. One of the simplest ones is a cone bombarded at perpendicular incidence. In cylindrical co-ordinates (x, ρ, ϕ), the cone surface is written as

$$x = C\rho\ ; \quad C > 0 \tag{12}$$

and $F_D(\mathbf{r})$ is given, in the notation of Equation 6, as

$$F_D(\mathbf{r}) = \frac{\nu}{(2\pi)^{3/2}\,\alpha\,\beta^2}\,e^{-(x-a)^2/(2\alpha^2)-\rho^2/(2\beta^2)}\ . \tag{13}$$

When Equations 12 and 13 are inserted into Equation 3, a fairly complex Bessel-integral is the result. To simplify the calculations, we directly consider those limits that have been considered previously.

Near the top ($x = \rho = 0$) we obtain

$$N_S(0)\,da = \phi\,A\,da\,\frac{\nu}{\sqrt{(2\pi)}}\,\frac{\alpha}{A^2}\,e^{-a^2/(2\alpha^2)} \left\{1 - \sqrt{(\pi/2)}\,\frac{C\,a\,\beta}{\alpha\,A}\,e^{C^2a^2\beta^2/(2A^2\alpha^2)}\,\mathrm{erfc}\left(\frac{C\,a\,\beta}{\sqrt{2}\,A\alpha}\right)\right\} \quad \ldots . \tag{14}$$

where

$$A = \sqrt{(\beta^2\,C^2 + \alpha^2)}\,. \tag{15}$$

Far out on the slope, for large values of ρ, we get

$$N_S(\infty)\,da = \phi\,A\,da\,\frac{\nu}{\sqrt{(2\pi)}}\,\frac{1}{A}\,e^{-a^2/(2A^2)} \tag{16}$$

which yields the ratio

$$\frac{N_S(0)}{N_S(\infty)} = \frac{\alpha}{A}\left\{e^{-(C^2a^2\beta^2)/(2A^2\alpha^2)} - \sqrt{(\pi/2)}\,\frac{C\,a\,\beta}{\alpha\,A}\,\mathrm{erfc}\left(\frac{C\,a\,\beta}{\sqrt{2}\,\alpha\,A}\right)\right\}. \tag{17}$$

This formula can be compared with Equation 9 that was derived for a ridge. However, the present ratio is usually substantially smaller. For example, for a cone with an opening angle of 45° ($C = 1$) the ratio (Equation 17) becomes ~ 0.2 with the numbers leading to Table I.

Dramatic effects are found for $C \gg 1$, i.e. for very narrow cones. In this case, Equation 3 reads ($C = \cot\,\psi$),

$$N_S(\rho)\,da = \phi\,A\,da\,\frac{\nu\,\alpha\,\sin^2\,\psi}{\sqrt{(2\pi)}\,\beta^2}\,e^{-\rho^2/(2\beta^2)} \left\{e^{-(x-a)^2/(2\alpha^2)} + \sqrt{(\pi/2)}\,\frac{x-a}{\alpha}\,\mathrm{erfc}\left(-\frac{x-a}{\alpha\sqrt{2}}\right)\right\} \quad C \gg 1\,. \tag{18}$$

This corresponds to Equation 11 for the ridge. The essential new feature is the factor $\sin^2\,\psi \ll 1$ in the numerator. Take, for example, the ratio of the regression speeds on top of a cone and on a plane at perpendicular incidence, i.e.

$$\frac{v_{\mathrm{top}}}{v_{\mathrm{plane}}} = \frac{\alpha^2}{\beta^2}\,\sin\,\psi\,.\left\{1 - \sqrt{(\pi/2)}\,\frac{a}{\alpha}\,e^{a^2/2\alpha^2}\,\mathrm{erfc}\left(\frac{a}{\sqrt{2}\,\alpha}\right)\right\}\ ; \quad \psi \text{ small} \tag{19}$$

which corresponds to Equation 10a, but *without* the factor $\sin\,\psi$ there. It is this factor that makes the top of a cone almost infinitely stable against sputtering. To be sure that this effect is not a

singular feature of a region of minute dimensions we also evaluate the ratio of the regression speed at $x = a$ ($\rho = (a/C) \ll a$) and that of a plane. Equation 18 yields

$$\frac{v(x=a)}{v_{\text{plane}}} = \frac{a^2}{\beta^2} \sin\psi \, e^{a^2/2\alpha^2} ; \quad x = a ; \quad \psi \text{ small} . \qquad (20)$$

Again this ratio is $\ll 1$. In order to understand qualitatively the results of Equations 19 and 20 one should appreciate that the top region of a narrow cone has lateral dimensions that are considerably smaller than that of a collision cascade. Such a region would normally – i.e. if it were imbedded in a plane, infinite target surface – be affected by a number of cascades covering an area of the order of $\pi\beta^2$. However, as it stands most of those cascades will miss the top of the cone and hit somewhere underneath. This will drastically reduce the sputtering effect.

For a ridge we had a factor of $\sin\psi$ in the sputtering yield per unit area; this is replaced by $\sin^2\psi$ for a cone. In the regression speed one factor of $\sin\psi$ is taken away. Thus while the top of a ridge had a regression speed that was only smaller by a factor of 2 to 3 than that of a plane (Table II), we get an order-of-magnitude effect in case of a cone or a cone-like structure. Note again that the effects will be *enhanced* when energy deposition functions valid for an infinite medium are replaced by those satisfying proper boundary conditions imposed by the location of the target surface.

4. Discussion

As was mentioned in the introduction, it is not the intention of the present work to rule out any of the suggested mechanisms for nucleation and growth of radiation-induced surface topography. We rather want to specify some of the consequences of the present considerations.

1. The present mechanism operates on a length scale of the order of the penetration depth of the ions. In those cases where observed structure has characteristic dimensions that are one or several orders of magnitude greater than the ion range, the present mechanism may at most be significant in determining the nucleation, not the growth. When the experimental resolution allows one to observe structures with dimensions of the order of the ion range, these dimensions should vary with ion energy in accordance with the ion range.

2. Surface smoothing by atom migration has been neglected in the present considerations. In those cases where migrational processes strongly act in the opposite direction, *lowering the temperature* will enhance the significance of the present mechanism. In this respect, the present mechanism is complementary to Hermanne's [4, 19], where nucleation takes place at defect clusters that arise by homogeneous nucleation of migrating point defects. The characteristic temperatures for the two mechanisms need not be identical nor even related. Thus, both mechanisms may act simultaneously. A key point for experimental investigations appears to be an indication of whether there exists an *upper* and/or a *lower* temperature limit for occurrence of surface topography.

3. Impurities have so far [8] been assumed to coagulate on certain positions, decreasing the sputtering yield locally, and thus giving rise to cone formation. In addition, impurities might inhibit (or enhance) migrational smoothing, and thus stimulate (or prevent) surface roughening by the present mechanism.

4. At sufficiently low temperatures, i.e. when no appreciable migrational smoothing takes place, a bombarded surface is expected to be rough on a scale determined by the ion range (and dose). The expected structures (furrows, cones, etc.) should be oriented such as to face the ion beam. Re-orienting the crystal surface should change the orientation of the observed surface structure. There appears to exist qualitative evidence to support this point experimentally [20, 21]. In view of the low ion energies employed in many experiments, the most dramatic effects of surface roughness may possibly have gone unnoticed so far. Spikes a few tens of Ångstrøms wide and ~ 100Å long may be extremely stable under ion bombardment (if stable at all), but may be difficult to detect and sensitive to mechanical and thermal treatment (replica). For polishing purposes [12, 22, 23] it may be advisable to avoid a well-collimated beam to hit the target constantly at one and the same direction.

5. It was mentioned previously that grooves are often observed around the bottom of a cone on an otherwise comparatively flat surface area [9]. The occurrence of these grooves may be explained by the mechanism sketched in Figs. 6 and 7, provided that the characteristic dimensions are reasonably close to the ion range. An alternative explanation [9, 12] involves sputtering by scattered ions and high-energy sputtered atoms.

Within the framework of collision cascade theory in an infinite medium, the two mechanisms appear to be very similar aspects of one basic mechanism. Analytic calculations including target surface effects at very oblique incidence may give further insight.

6. Although it has been asserted that the present mechanism can be responsible for the nucleation of surface topography, this cannot be literally true. As it stands, Equation 3 provides an instability, but requires small irregularities before enhancement is possible. Such irregularities can be at a smaller scale than the ion range. They may be provided by craters left behind an exceptionally violent sputtering event (note that fluctuations of the sputtering yield may be substantial [17]), the trace behind a sputtered cluster [10], a region of high sputtering yield because of lattice damage [4] or a small island of impurities [8]. The present mechanism probably provides a useful link between the events taking place on an atomic scale and those features that can be predicted from the *macroscopic* variation of the sputtering yield with the direction of incidence [5, 6].

7. It is evident that pronounced surface topography can influence the magnitude of the total sputtering yield. Within the present description, the main effects are an *increase* in yield as compared to a flat surface because of an increase in surface area, and a *decrease* in yield because of increased redeposition for oblique ejection. The deposited-energy function in Equation 1 is less sensitive to surface topography, since it is an average according to Equation 3 over the whole surface area. This point has already been mentioned in [13]. It is most reasonable to assume that surface topography is responsible for part of the dose effects observed in recent sputtering-yield measurements [24]. This is consistent with the experience that the observed variation of the yield with ion energy, type, and angle of incidence is predicted well by the theory [13], while the absolute magnitude depends on the history of the target.

Acknowledgements

My sincere thanks are due to all those, especially Mike Thompson and Nelly Hermanne, who kept telling me that surfaces need not be flat.

References

1. R. BEHRISCH, *Erg. ex. Nat. wiss.* **35** (1964) 295.
2. G. CARTER and J. S. COLLIGON, "Ion Bombardment of Solids" (Heinemann, London, 1968).
3. B. NAVINSEK, *in* "Physics of Ionized Gases", ed. by M. V. Kurepa (Institute of Physics, Belgrade, 1972) p. 221.
4. N. HERMANNE and A. ART, *Rad. Eff.* **5** (1970) 203.
5. A. D. G. STEWART and M. W. THOMPSON, *J. Mater. Sci.* **4** (1969) 56.
6. M. J. NOBES, J. S. COLLIGON, and G. CARTER, *ibid* **4** (1969) 730; *ibid* **6** (1971) 115; C. CATANA, J. S. COLLIGON, and G. CARTER, *ibid* **7** (1972) 467.
7. I. A. TEODORESCU and F. VASILIU, *Rad. Eff.* **15** (1972) 101.
8. G. K. WEHNER and D. J. HAJICEK, *J. Appl. Phys.* **42** (1971) 1145.
9. I. H. WILSON and M. W. KIDD, *J. Mater. Sci.* **6** (1971) 1362.
10. G. STAUDENMEIER, *Rad. Eff.* **13** (1972) 87.
11. W. HEILAND and E. TAGLAUER, *ibid* (in press).
12. A. R. BAYLY, *J. Mater. Sci.* **7** (1972) 404.
13. P. SIGMUND, *Phys. Rev.* **184** (1969) 383.
14. P. SIGMUND and J. B. SANDERS, *in* Proc. of the Int. Conf. on Application of Ion Beams to Semiconductor Technology, Editions Ophrys, Paris (1967), p. 215; K. B. WINTERBON, P. SIGMUND, and J. B. SANDERS *Mat. Fys. Medd. Dan. Vid. Selsk.* **37** (14) (1970); P. SIGMUND, M. T. MATTHIES, and D. L. PHILLIPS, *Rad. Eff.* **11** (1971) 34; K. B. WINTERBON, *Rad Eff.* **13** (1972) 215.
15. P. SIGMUND, *Rev. Roum. Phys.* **17** (1972) 1079; P. SIGMUND, as [3], p. 137.
16. J. BØTTIGER, J. A. DAVIES, P. SIGMUND, and K. B. WINTERBON, *Rad. Eff.* **11** (1971) 69.
17. J. E. WESTMORELAND and P. SIGMUND, *ibid* **6** (1971) 187.
18. J. LINDHARD, V. NIELSEN, M. SCHARFF, and P. V. THOMSEN, *Mat. Fys. Medd. Dan. Vid. Selsk.* **33** (10) (1963)
19. N. HERMANNE, *Rad. Eff.* (in press).
20. J. J. TRILLAT, *in* "Le Bombardement Ionique", Ed. du Centre National de la Recherche Scientifique, Paris 1962, p. 13.
21. M. P. HAYMANN and C. WALDBURGER, *ibid* p. 205.
22. M. NAVEZ, C. SELLA, and D. CHAPEROT, *ibid* p. 233.
23. A. R. BAYLY and P. D. TOWNSEND, *J. Phys. D* **5** (1972) L 103.
24. H. H. ANDERSEN and H. BAY, *Rad. Eff.* **13** (1972) 67.

Received 7 March and accepted 28 March 1973.